J. Nucl. Phys. Mat. Sci. Rad. A. Vol. 9, No. 1 (2021), pp.47–53

CHITKARA

Journal of Nuclear Physics, Material Sciences, Radiation and Applications
Journal homepage: https://jnp.chitkara.edu.in/

Comparative Analysis of ^{13,14}C Induced Reactions on ^{232}Th Target

Manpreet Kaur[1*], BirBikram Singh[2] and Manoj K. Sharma[3]

[1]*Department of Physics, Sri Guru Granth Sahib World University, Fatehgarh Sahib, Punjab - 140407, India*

[2]*Department of Physics, Akal University, Talwandi Sabo, Bathinda, Punjab - 151302, India*

[3]*School of Physics and Materials Science, Thapar Institute of Engineering & Technology, Patiala, Punjab - 147004, India*

[*]manpreetphysics95@gmail.com (Corresponding Author)

ARTICLE INFORMATION

Received: January 15, 2021
Accepted: April 15, 2021
Published Online: August 31, 2021

Keywords:
Compound nucleus, Isotopes, Dynamical Cluster Decay Model (DCM), Preformation probability

DOI: 10.15415/jnp.2021.91009

ABSTRACT

We have investigated the pairing and magicity effect in context of a comparative study of ^{13,14}C induced reactions on ^{232}Th target at energies in the vicinity of Coulomb barrier. The fission distribution and related properties are explored in terms of the summed-up preformation probabilities. The barrier-penetrability is found to be higher for fragments emitted from ^{246}Cm* formed in ^{14}C+^{232}Th reaction than those emitted in the fission of ^{245}Cm*, leading to higher magnitude of cross-section for earlier case. The DCM calculated fusion-fission cross-sections using ΔR=0 fm are normalised to compare with the available experimental data. The calculations are done for spherical shape of fragments and it will be of further interest to explore the fission mass distribution after the inclusion of deformations.

1. Introduction

Heavy ion induced reactions has been a topic of interest among the nuclear science community as they provide a wonderful tool to investigate the behaviour of finite and infinite nuclear matter. The proper selection of the target projectile combination plays a crucial role to synthesize new nuclei as the non-compound nucleus phenomena like quasi-fission (QF) may hinder the complete amalgamation of colliding partners. With the availability of high intensity beams of a variety of heavy ions, experimental and theoretical investigations have taken a huge jump during last few decades. The nuclear properties of the projectile and target are manifested in associated reaction mechanism. The role of neutron enrichment of the projectile on fusion-fission mechanism and competing reaction processes can be understood through the comparative study of the reactions induced by isotopic chain of projectiles.

Earlier, we investigated the fusion-fission of reactions involving bombardment of ^{12,15}C projectiles on ^{232}Th target [1] within dynamical cluster decay model (DCM) of Gupta and collaborators [1-9]. In this paper, we want to extend our study to compare the influence of two other isotopes of carbon, ^{13,14}C incident on the same target ^{232}Th. Thus, the different aspects involved in decay of isotopic compound nuclei $^{244-247}$Cm* could be explored at centre of mass energies where experimental data is available [10, 11]. It is relevant to mention here that DCM has been successfully applied to understand the fusion mechanism in mid-mass composite systems $^{67-69,73-75}$As* formed in collision of $^{39-41,45-47}$K isotopes with ^{28}Si and fusion enhancement with neutron number at near-barrier energies was studied [8]. The yields of various light particles (LPs) and intermediate mass fragments (IMFs) calculated within DCM formalism in decay of lighter compound nuclei $^{26-29}$Al* formed with different isotopes of Oxygen and Boron, are consistent with experimental data [6]. For the heavy mass region, the compound nucleus (CN) often undergoes binary fission due to its high fissility. The reaction dynamics of Pt isotopes and reversal of behavior of fission fragments, i.e., from asymmetric to symmetric, with a decrease in the N/Z ratio was observed within framework of DCM, which may be ascribed to neutron number [4]. Thus, the reaction mechanism of fusion and subsequent decay into fission fragments is strongly influenced by neutron content of the reaction partners particularly with magic character of the projectile. In present work, we have compared the decay pattern of ^{245}Cm* formed in a reaction having one of the reaction partners with odd number of neutrons (^{13}C), and

©Author(s) 2021. This article is published with open access at https://jnp.chitkara.edu.in.
ISSN No.: 2321-8649(Print) ISSN No.: 2321-9289(Online); Registration No. : CHAENG/2013/51628

$^{246}Cm^{*}$ where isotope of same element with magic number of neutrons is participating in the reaction. The behavior of fragmentation potential and preformation probability is analyzed to obtain a clear picture of the dynamics involved in both the reactions using neck-length parameter of DCM, ΔR=0 fmby considering spherical shape of decay fragments. The structure of the paper is as follows. In Section 2, a brief methodology of DCM is given. In Section 3, the results and discussions of the calculations are presented. Finally, conclusions are summarised in the Section 4.

2. Methodology

The dynamical cluster decay model (DCM) is based on the Quantum mechanical fragmentation theory (QMFT) to study decay of hot and rotating compound nuclei. DCM considers all decay products as dynamical mass motions of preformed fragments or clusters through the interaction barrier. It is worked out in terms of:

(i) The mass asymmetries $\eta = \frac{(A_1 - A_2)}{(A_1 + A_2)}$.

where A_1 and A_2 denote the mass of fusing nuclei or of the fission fragments which characterizes nucleon- division (or -exchange) between the outgoing fragments.

(ii) Relative separation between the two nuclei R, which characterizes the transfer of kinetic energy of the incoming channel ($E_{c.m.}$) to internal excitation or kinetic energy of the outgoing fragments.

DCM defines the CN-decay cross section, including the temperature and angular momentum contribution, in terms of partial waves, as

$$\sigma = \sum_{\ell=0}^{\ell_{max}} \sigma_\ell = \frac{\pi}{k^2} \sum_{\ell=0}^{\ell_{max}} (2\ell+1) P_0 P \text{ ,with } k = \sqrt{\frac{2\mu E_{C.M}}{\hbar^2}} \tag{1}$$

Here P_0(preformation probability), refers to η-motion and P (the penetrability), refers to R-motion.

The fragments are pre-born inside the parent nucleus with relative preformation probability, P_0, given by

$$P_0 = \left|\Psi(\eta(A))\right|^2 \sqrt{B_{\eta\eta}} \frac{2}{A^*_{CN}} \tag{2}$$

It is the solution of stationary Schrodinger equation in η co-ordinate calculated at fixed first turning point R = R_a,

$$\left\{ -\frac{\hbar^2}{2\sqrt{B_{\eta\eta}}} \frac{\partial}{\partial\eta} \frac{1}{\sqrt{B_{\eta\eta}}} \frac{\partial}{\partial\eta} + V_R(\eta) \right\} \Psi_R^{(\nu)}(\eta) = E_R^{(\nu)} \Psi_R^{(\nu)}(\eta) \tag{3}$$

with ν = 0, 1, 2, 3……. referring to ground state (ν = 0) and excited states (ν = 1, 2, 3, …) solutions, where mass parameters $B_{\eta\eta}$ are the smooth classical hydrodynamical masses [12, 13].

Here,

$$R_a(T,\eta,\alpha) = R_t(T,\eta,\alpha) + \Delta R(\eta,T) \tag{4}$$

where $R_t(T,\eta,\alpha) = R_1(T,\eta,\alpha_1) + R_2(T,\eta,\alpha_2)$ and $\Delta R(\eta,T)$ is neck length parameter that assimilates neck formation effects and is taken to be, $\Delta R = 0\,fm$, in the present work.

The temperature dependent nuclear radii $R_i(T)$ for the equivalent spherical nuclei take the form

$$R_i(T) = \left[1.28A_i^{1/3} = -0.76 + 0.8A_i^{1/3}\right]\left(1 + 0.0007T^2\right) \tag{5}$$

The structure effects of the CN enter via collective fragmentation potential, $V_R(\eta, T)$ which is calculated within Strutinsky renormalization procedure $(B.E = V_{LDM} + \delta U)$ [14], T-dependent liquid drop energy V_{LDM} is taken from Davidson et al. [15] and empirical shell corrections δU from Myres and Swiatecki [16] and including T-dependence in the nuclear proximity (V_p), Coulomb (V_C) and angular momentum dependent potential (V_ℓ),

$$V_R(\eta,T) = \sum_{i=1}^{2} \left[V_{LDM}(A_i,Z_i,T) + (\delta U_i) e^{\left(-\frac{T^2}{T^2}\right)} \right] + V_C(R,Z_i,T) + V_P(R,A_i,T) + V_\ell(R,A_i,T) \tag{6}$$

Once the fragments are preformed, their penetrability P can be calculated by using WKB integral, according to which

$$P = \exp\left[-\frac{2}{\hbar} \int_{R_a}^{R_b} \left\{ 2\mu \left[V(R) - Q_{eff} \right] \right\}^{\frac{1}{2}} dR \right] \tag{7}$$

with the first and second turning points R_a and R_b satisfying $V(R_a) = V(R_b) = Q_{eff}$

3. Results and Discussions

The fragmentation behavior and fission mass distribution are analysed using dynamical cluster decay model (DCM). We have studied the effect of neutron addition or isotopic effect via study of decay of $^{245}Cm^{*}$ and $^{246}Cm^{*}$ populated in ^{13}C and ^{14}C induced reactions respectively on target ^{232}Th at similar values of $E_{c.m.}$ around 69 MeV where experimental data is available [10, 11].

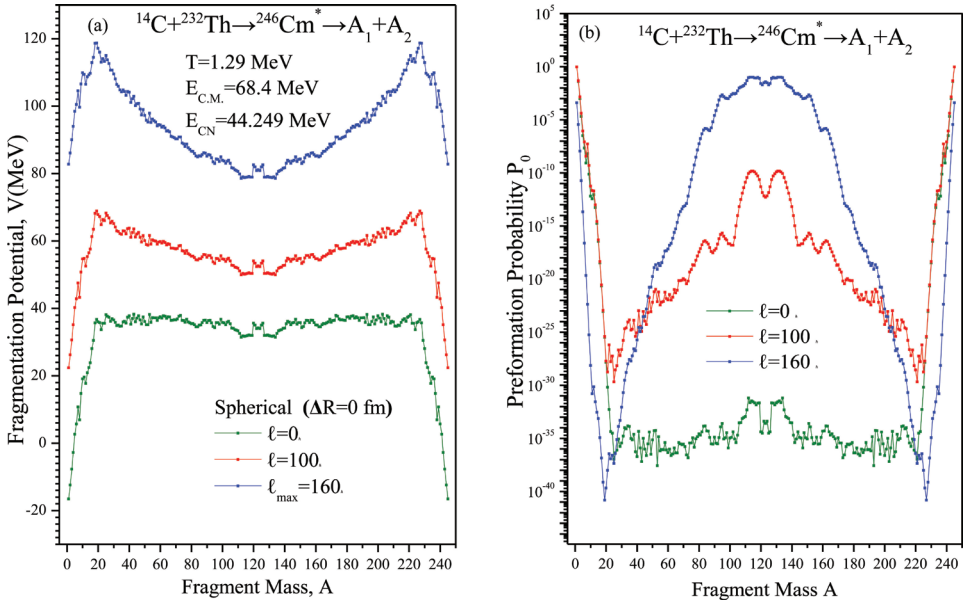

Figure 1: The (a) fragmentation potential, V(MeV) (b) preformation probability, P_0 as a function of fragment mass forthe decay of $^{246}Cm^{*}$.

Fig. 1(a) presents the variation of fragmentation potential, V(MeV) as a function of fragment mass for the decay of $^{246}Cm^{*}$ at T=1.29 MeV, corresponding to excitation energy, $E^{*}_{CN} = 44.249$ MeV at ℓ=0 $\hbar$, ℓ=100 $\hbar$ and ℓ_{max}=160 $\hbar$. The calculations are done with value of neck-length parameter, ΔR=0 fm considering the spherical shape of nuclei. We observe that Light Particles (LPs: A≤4; Z≤2) are minimized at ℓ=0 $\hbar$ whereas with the inclusion of angular momentum effects, FF fragments (A=(A_{CN}/2)±20) start competing gradually at higher ℓ-values. It is clear that magnitude of fragmentation potential for intermediate mass fragments (IMFs: 5≤ A≤20) is more in comparison to other emission fragments at lower as well as higher ℓ-values, thus they are not energetically favoured in the decay process. The preformation probabilities follow the inverse trend of fragmentation profile as analysed through the variation of relative preformation probabilities with the fragment mass at same ℓ-values in Figure 1(b). It is observed that the contribution of LPs and IMFs goes on decreasing with the increase in the value of angular momentum but FF fragments are strongly preformed at higher ℓ-values. Thus, the shape of preformation curve changes from U to W under the effect of rotational energy.

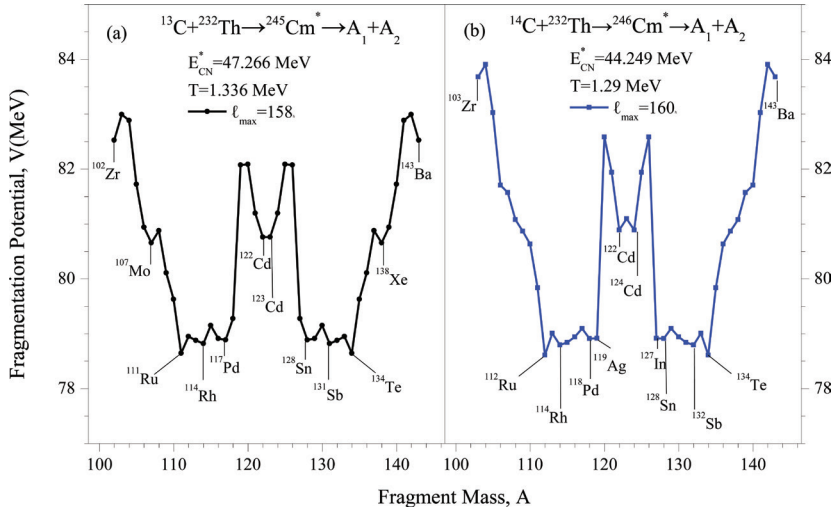

Figure 2: The fragmentation potential of FF fragments as a function of fragment mass at l_{max} ($\hbar$) for the decay of compound nuclei (a) $^{245}Cm^{*}$ (b) $^{246}Cm^{*}$.

For the present work, we are interested in the fusion-fission window where the experimental data of cross-sections is available [10, 11]. The fragmentation potential for FF fragments is illustrated in Fig. 2 for both the compound nuclei $^{245}Cm^*$ and $^{246}Cm^*$ at their respective ℓ_{max}-values, which show similar behaviour. The value of ℓ_{max} is critical value of angular momentum corresponding to vanishing of LPs cross section $\sigma_{LP} \rightarrow 0$. The $\ell_{max}=158\,\hbar$ for $^{245}Cm^*$ and $\ell_{max}=160\,\hbar$ for $^{246}Cm^*$. The pattern behaviour remains almost same as most of the minimized fragments are similar.

Furthermore, the contribution of different mass fragments is explored in Fig. 3 where the summed-up preformation probability of FF fragments, $\sum P_0(\ell = 0\ \hbar$ to $\ell_{max})$ values are plotted. There are minute changes in $\sum P_0$ with symmetric and near- symmetric mass fragments (SMFs and nSMFs: $A = (A_{CN}/2) \pm 4$) getting slightly higher values for heavier isotope and far asymmetric mass fragments (aSMFs) are further stretched down in the tails. The preformation probability carries the nuclear structure information. The added neutron in case of ^{14}C is making the projectile magic, N=8 and the P_0 values does not the vary much for transition from ^{13}C to ^{14}C induced reactions. Although, in our earlier investigation of decay of other isotopes of Cm populated as Compound nuclei in $^{12,15}C+^{232}Th$ reactions at similar excitation energies, we observed a significant change in the $\sum P_0(\ell = 0\ \hbar$ to $\ell_{max})$ values for symmetric and near-symmetric decay fragments as we move from $^{244}Cm^*$ to more neutron-rich CN, $^{247}Cm^*$ which was populated with halo projectile, ^{15}C [9]. It clearly indicates that the removal/addition of neutrons in projectile plays significant role in the underlying reaction dynamics.

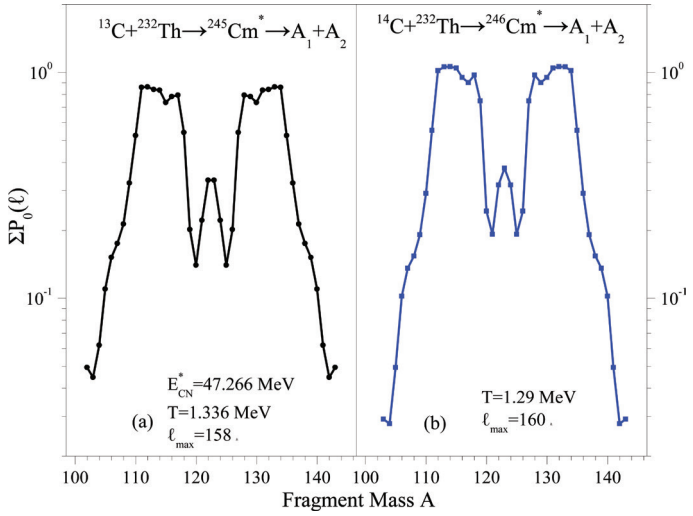

Figure 3: The summed-up preformation probability of FF fragments, $\sum P_0(\ell = 0\ \hbar$ to $\ell_{max})$ as a function of A for the decay of compound nuclei (a) $^{245}Cm^*$ (b) $^{246}Cm^*$.

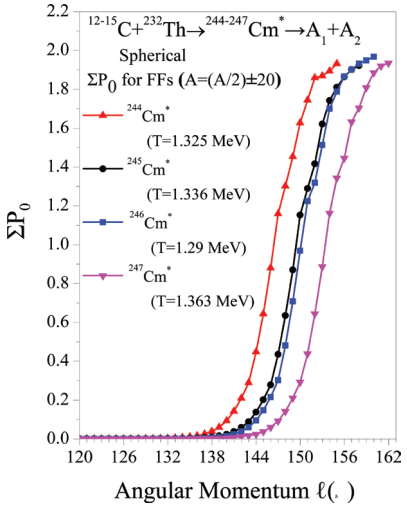

Figure 4: The $\sum P_0$ of FF fragments, as a function of angular momentum $\ell(\hbar)$ for the decay of compound nuclei under study.

The role of angular momentum in the decay dynamics is explored through summed-up preformation probability of FF fragments, $\sum P_0(A=A_{CN}/2\pm 20)$ as a function of angular momentum $\ell(\hbar)$ in Fig. 4. The curves for preformation probability of FF fragments for ^{13}C and ^{14}C induced reactions lie in between that of ^{12}C and ^{15}C as expected. The analysis depicts that curve shift to higher ℓ values from ^{12}C to ^{13}C having 6 and 7 neutrons, respectively due to the fact that the interaction of unpaired neutron (in case of ^{13}C) will be more probable with the ^{232}Th target. But the values do not vary much from ^{13}C to ^{14}C which can be attributed to the magic neutron number N=8 in case of ^{14}C and when we move ahead from ^{14}C to ^{15}C having unpaired neutron, the increase is again significant as the last valence neutron is considered to be lying outside the closed neutron shell. Thus, the effect is more in transition from paired to unpaired neutron nuclei as compared to unpaired to adjacent paired neutron nuclei.

The preformed fragments are emitted as decay products after their subsequent penetration through the interaction potential barrier. The ℓ-summed penetration probability of all the preformed fragments is represented in Fig. 5 as a function of fragment mass. Interestingly, the penetration probabilities, $\Sigma P(\ell = 0\ \hbar$ to $\ell_{max})$, are quite higher in case of $^{246}Cm^*$ as compared to $^{245}Cm^*$ for the whole range of FF fragments, leading to higher magnitude of fusion-fission cross-sections. The $\Sigma P(\ell)$ has similar order of magnitude for all the fragments in fusion-fission region for decay of $^{245}Cm^*$, but for the case of $^{246}Cm^*$, $\Sigma P(\ell)$ contributes in evolution of cross-section structure.

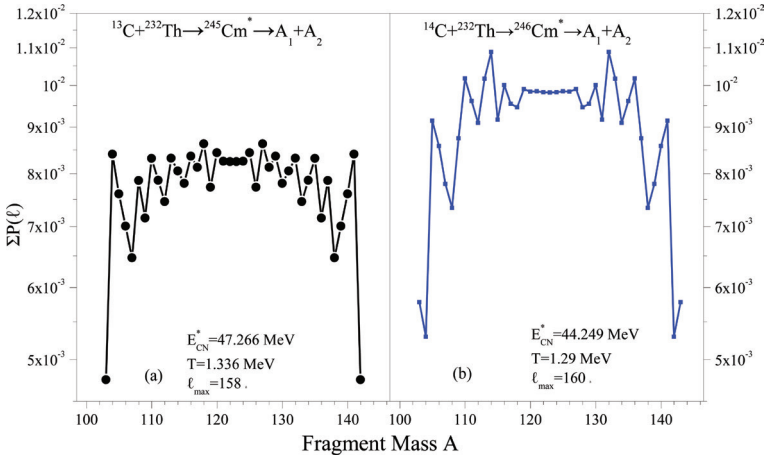

Figure 5: The summed-up penetration probability of FF fragments, $\Sigma P(\ell = 0\ \hbar$ to $\ell_{max})$ as a function of A for the decay of compound nuclei (a) $^{245}Cm^*$ (b) $^{246}Cm^*$.

In Fig. 6, the normalized values of fusion-fission cross-section () are plotted to get an estimate of the mass distribution of FFs. We notice that the trend of variation of is similar to that of $\Sigma P_0(\ell)$, and the peak at A=114 and its complimentary fragment having A=132 are reinforced due to combined contribution of preformation and penetration probabilities plotted in Figs. 3 and 5. Thus, shows the combined effect of ΣP_0 and ΣP and the overall cross-section values get modified according to the product of these two quantities. The DCM calculated cross-sections are quite low for SMFs and nSMFs as compared to neighboring fragments which seem to be dominant decay channel in the considered nuclei.

The normalized values of σ_{FF}^{DCM} is compared with experimental data in Table 1. We will try to improve the comparison with exact fitting of the neck-length parameter in subsequent work. The deformations and orientation degrees of freedom of QMFT will be considered in the next step along with the role of neck-length parameter, ΔR within DCM formalism for further understanding the underlying dynamics of the reactions.

Table 1: The characteristic quantities of considered reactions along with DCM calculated cross-sections, compared with experimental data.

S. No.	Reaction	$E_{C.M.}$(MeV)	(MeV)	T (MeV)	$\ell_{max}(\hbar)$	DCM (Spherical) (mb) with ΔR=0 fm(Normalised values)	Expt. σFF(mb)
1	$^{13}C+^{232}Th\rightarrow^{245}Cm^*\rightarrow A_1+A_2$	69.7	47.266	1.336	158	515.91	549±13
2	$^{14}C+^{232}Th\rightarrow^{246}Cm^*\rightarrow A_1+A_2$	68.4	44.249	1.29	160	703.11	581±8

Summary

The dynamical cluster decay model (DCM) has been applied for comparative analysis of ^{13}C and ^{14}C induced reactions on ^{232}Th target at similar centre of mass energies ($E_{c.m.}$). We considered the spherical shape of nuclei, with $\Delta R=0$ fm to calculate the normalized values of fusion-fission cross-section (σ_{FF}^{DCM}).The dynamical collective clusterisation process, used in DCM seems an effective tool to predict mass distribution of decay products of compound systems produced in low energy heavy ion collisions. The influence of angular momentum on fragmentation potential and correspondingly on preformation probability is addressed. For both the considered compound nuclei, peaks are found at similar fragment mass values of fission fragments. It would be of further interest to investigate the decay patterns of these isotopic compound nuclei by taking into account the effect of other factors like that ofdeformations and orientation degrees of freedom.

References

[1] M. Kaur, B. B. Singh and M. K. Sharma, AIP Conference Proceedings **2532**, 050031 (2021). https://doi.org/10.1063/5.0053354

[2] R. K. Gupta, R. Kumar, N. K. Dhiman, M. Balasubrmaniam, W. Scheid and C. Beck, Phys. Rev. C **68**, 014610 (2003). https://doi.org/10.1103/PhysRevC.68.039901

[3] B. B. Singh, M. K. Sharma and R. K. Gupta, Phys. Rev. C. **77**, 054613 (2008). https://doi.org/10.1103/PhysRevC.77.054613;
B. B. Singh, PhD Thesis, Thapar University, Patiala (2009).

[4] D. Jain, R. Kumar, M. K. Sharma and R. K. Gupta, Phys. Rev. C. **85**, 024615 (2012). https://doi.org/10.1103/PhysRevC.85.024615

[5] B. B. Singh et al., Jour. of Phys. Conf. Proc. **569**, 012030 (2014). https://doi.org/10.1088/1742-6596/569/1/012030
Jour. of Phys. Soc. Conf. Proc **6**, 030001 (2014). https://doi.org/10.7566/JPSCP.6.030001
EPJ Web Conf. **86**, 00048 (2015). https://doi.org/10.1051/epjconf/20158600048
EPJ Web Conf. **86**, 00049 (2015). https://doi.org/10.1051/epjconf/20158600049
Applied Science Letters **02**, 114 (2016). https://doi.org/10.1002/wea.2713

[6] M. Kaur et al., Phys. Rev. C **92**, 024623 (2015). https://doi.org/10.1103/PhysRevC.92.024623
Nucl. Phys. A **980**, 67 (2018). https://doi.org/10.1016/j.nuclphysa.2018.09.079
Nucl. Phys. A **969**, 14 (2018). https://doi.org/10.1016/j.nuclphysa.2017.09.014
AIP Conf. Proc. **2220**, 130059 (2020). https://doi.org/10.1063/5.0005461

[7] M. Kaur et al., Phys. Rev. C **95**, 014611 (2017). https://doi.org/10.1103/PhysRevC.95.014611
AIP Conf. Proc. **1953**, 140113 (2018). https://doi.org/10.1063/1.5033288
Phys. Rev. C **99**, 014614 (2019). https://doi.org/10.1103/PhysRevC.99.014614

[8] R. Kaur et al., Phys. Rev. C **98**, 064612 (2018). https://doi.org/10.1103/PhysRevC.98.064612
Phys. Rev. C **101**, 034614 (2020). https://doi.org/10.1103/PhysRevC.101.034614
Phys. Rev. C **101**, 044605 (2020). https://doi.org/10.1103/PhysRevC.101.044605
AIP Conf. Proc. **2220**, 130036 (2020). https://doi.org/10.1063/5.0001455

[9] M. Kaur, S. Kaur and B. B. Singh, AIP Conf. Proc. **1953**, 140098 (2018). https://doi.org/10.1063/1.5033273
M. Kaur, S. Kaur, B. B. Singh and M. K. Sharma, AIP Conf. Proc. **2220**, 130059 (2020). https://doi.org/10.1063/5.0005461

[10] J. C. Mein et al., Phys. Rev. C **55**, R995(R) (1997). https://doi.org/10.1103/PhysRevC.55.R995

[11] M. Alcorta, K. E. Rehm, B. B. Back et al., Phys. Rev. Lett. **106**, 172701 (2011). https://doi.org/10.1103/PhysRevLett.106.172701

[12] J. Maruhn and W. Greiner, Phys. Rev. Lett. **32**, 548 (1974). https://doi.org/10.1103/PhysRevLett.32.548

[13] R. K. Gupta, W. Scheid and W. Greiner, Phys. Rev. Lett. **35**, 353 (1975). https://doi.org/10.1103/PhysRevLett.35.353

[14] V. M. Strutinsky, Nucl. Phys. A **95**, 420 (1967). https://doi.org/10.1016/0375-9474(67)90510-6

[15] N. J. Davidson, S. S. Hsiao, J. Markram, H. G. Miller and Y. Tzeng, Nucl. Phys. A **570**, 61 (1994). https://doi.org/10.1016/0375-9474(94)90269-0

[16] W. Myers and W. J. Swiatecki, Nucl. Phys. **81**, 1 (1966). https://doi.org/10.1016/0029-5582(66)90639-0

Journal of Nuclear Physics, Material Sciences, Radiation and Applications

Chitkara University, Saraswati Kendra, SCO 160-161, Sector 9-C, Chandigarh, 160009, India

Volume 9, Issue 1 **August 2021** **ISSN 2321-8649**

Copyright: [© 2021 Manpreet Kaur, BirBikram Singh and Manoj K. Sharma] This is an Open Access article published in Journal of Nuclear Physics, Material Sciences, Radiation and Applications (J. Nucl. Phy. Mat. Sci. Rad. A.) by Chitkara University Publications. It is published with a Creative Commons Attribution- CC-BY 4.0 International License. This license permits unrestricted use, distribution, and reproduction in any medium, provided the original author and source are credited.